FINITE ELEMENT MODELING OF HYBRID ADDITIVE MANUFACTURING BY LASER SHOCK PEENING

M.P. Sealy[a], G. Madireddy[a], C. Li[b], Y.B. Guo[b]

[a] Dept. of Mechanical and Materials Eng., University of Nebraska, Lincoln, NE 68588, U.S.A.
[b] Dept. of Mechanical Eng., The University of Alabama, Tuscaloosa, AL 35401, U.S.A.

Abstract

Hybrid manufacturing has traditionally targeted efficiency and productivity as improvement criteria. However, the advent of additive manufacturing to print functional parts has expanded the possibilities for a hybrid approach in this field. Hybrid additive manufacturing is the combination of two or more manufacturing processes or materials that synergistically affect the quality and performance of a printed part. Hybrid additive manufacturing allows for advancements in material properties beyond efficiency and productivity. Mechanical, physical, and chemical properties can be designed and printed. The purpose of this study was to model a hybrid additive manufacturing process to investigate the resulting mechanical properties. Laser shock peening (LSP) was coupled with selective laser melting in a 2D finite element simulation in Abaqus to quantify the resulting residual stress fields. The effects of peak pressure and layer thickness were studied when coupling laser shock peening with selective laser melting.

Keywords: hybrid, SLM, laser shock peening, Ti64, residual stress

1. Introduction

In today's manufacturing industry, the continuous requirement of high quality materials with preferential mechanical properties requires the use of various manufacturing techniques. Additive manufacturing (AM) is a promising method to avoid several limitations of conventional manufacturing processes; however, AM still presents certain challenges in terms of manufacturing high quality parts. For example, thermal loads in metal AM cause tensile residual stresses [1] which can be detrimental to fatigue. Furthermore, surface finish is poor in some AM processes such as directed energy deposition. An alternative to conventional AM is hybrid-AM. A hybrid approach combines two or more manufacturing processes that synergistically affect the quality and performance of a part [2]. The quality is superior to that achieved by an individual process. A common example of hybrid-AM combines additive manufacturing with subtractive machining [3-12]. In doing so, a workpiece attains a superior surface finish during printing on internal and external surfaces. Other areas of hybrid-AM include rolling [13-16] and laser re-processing[17-19].

Hybrid additive manufacturing is an emerging area of research. Sreenathbabu and Karunakaran investigated hybrid adaptive layer manufacturing which incorporates printing, heat treating, and machining each layer for rapid tool production [20]. Heat treating relieves stress and strengthens the tool. After the heat treatment, the layer is machined from near net shape to the final dimensions.

Shiomi et al. used selective laser melting followed by heat treatment [1]. Strain gages were used to calculated residual stresses after SLM. They observed that large tensile stresses remain on the surface after SLM and found that heat treating reduced the tensile stresses by approximately 70%. Qian et al. proposed hybrid plasma-laser deposition manufacturing (PLDM) which combines the heat sources of the plasma arc beam and laser [21]. They observed that the physical properties of the surface coating were better than plasma deposition manufacturing alone. To the authors knowledge, the only known hybrid-AM simulation was by Zhou et al. [16]. They simulated the microstructural evolution from a hybrid deposition and micro-rolling process to study the effect of rolling on dynamic recrystallization. Others have investigated hybrid welding processes [22-24].

The objective of this paper is to propose a new manufacturing process which combines laser shock peening (LSP) and selective laser melting for hybrid additive manufacturing. LSP is a surface treatment used to improve the mechanical properties of a material. The laser irradiates a target and produces a shock wave that plastically deforms the workpiece. This shock wave hardens and strengthens the surface. The effects of LSP can extend several millimeters below the surface.

Many researchers have investigated the effect of LSP on different materials and confirmed that LSP can improve the properties by inducing compressive residual stresses [25-28]. Additive manufacturing is a process of joining materials to make parts from a 3D model, usually layer upon layer, as opposed to subtractive manufacturing and formative manufacturing methodologies. Additive manufacturing processes, such as selective laser melting (SLM), selective laser sintering (SLS), and electron beam melting (EBM), can produce products with tensile residual stresses [1,29]. It is hypothesized that these tensile stresses can be altered by employing laser shock peening between printed layers. With the change in residual stresses and increased hardness, the performance of a part can be improved or manipulated. This hybrid additive manufacturing approach enables one to design and print preferential mechanical properties for specific applications. In this study, hybrid additive manufacturing via laser shock peening was modeled in Abaqus. The effects of layer thickness and peening pressure on the residual stresses were studied.

2. Finite Element Model

2.1 Model Design

A series of two-dimensional finite element models were developed in Abaqus Standard to simulate consecutive layers of selective laser melting (SLM) followed by laser shock peening (LSP) on Ti64. The simulation was based on the work from Sealy and Guo [30,31] and Chao and Guo [32]. The objective was to model a hybrid additive manufacturing process, i.e. SLM and LSP, to determine the effect of successive printed layers on the enhanced mechanical properties from LSP. The simulation procedure applied a moving heat flux in a thermal model and imported the resulting temperatures into a stress model. Importing temperatures accounted for thermal strains caused by the heat flux. After allowing the temperatures to cool for 5 seconds, laser shock peening was applied to each printed layer via a shock pressure load. This process was repeated for each printed layer.

The workpiece was divided into four parts: substrate, layer 1, layer 2, and layer 3, see Fig. 1. The substrate was 4 mm (length) by 1 mm (thickness). Each layer was 2 mm long. Three different layer thicknesses were investigated: 100 µm, 300 µm, and 600 µm. In each model, three layers were printed and subsequently peened. Layer build-up was accomplished by first deactivating the entire mesh and then activating each layer in each active heat flux step. The thermal model used 4-node linear diffusive heat transfer elements (DC2D4), and the stress model used 4-node bilinear plain stress elements with reduced integration (CPS4R). Plain stress elements were chosen as one single printed line was assumed to be a thin body.
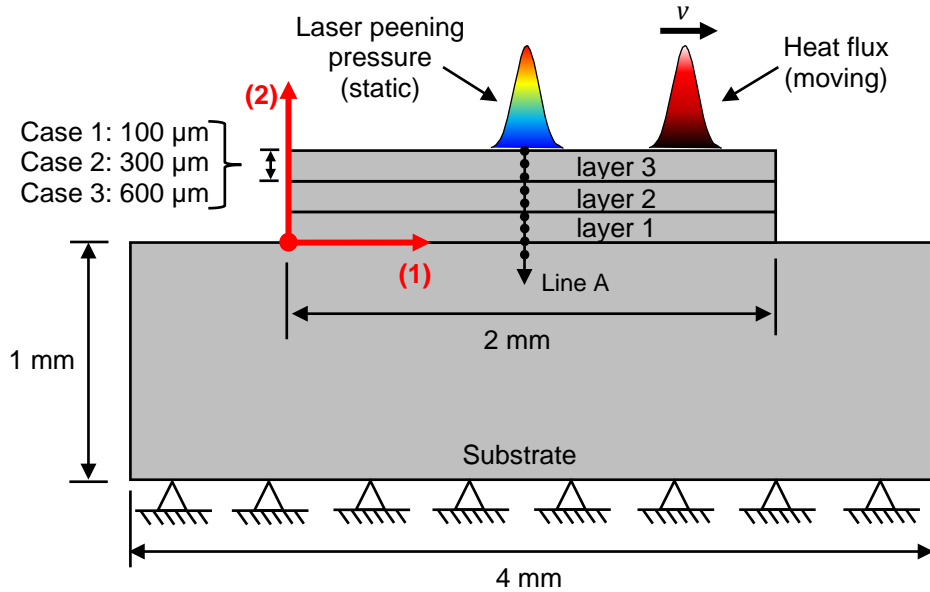

Fig. 1 Two-dimensional model of hybrid additive manufacturing.

2.2 Material Model

The material used for this model was Ti64. The physical and thermal properties as well as the temperature dependent thermal and mechanical properties used in the analysis are shown in Tables 1-3 [33-36]. At room temperature, the elastic modulus was 110 GPa and the yield strength was 910 MPa. At 1655 °C, the elastic modulus and yield strength decreased to 10% of that at room temperature. Since laser peening involves high strain rates (on the order of 10^6) that significantly affects the flow stress, future studies will incorporate more complex material models such as Johnson-Cook or an Internal State Variable (ISV) plasticity model based on the BCJ model to capture such rate dependent effects.

Table 1 Physical and Thermal Properties of Ti64

Density	(kg/m³)	4428
Latent heat	(J/kg)	365200
Solidus Temp	(°C)	1605
Liquidus Temp	(°C)	1655

Table 2 Temperature Dependent Thermal Properties of Ti64

Temp. (°C)	Specific Heat (J/Kg-K)	Temp. (°C)	Thermal Conductivity (W/m-K)	Temp. (°C)	Thermal Expansion (°C^{-1})
20	580	27	7.2	20	1.28×10^{-5}
205	610	100	8.2	538	1.40×10^{-5}
425	670	200	9.4	927	1.62×10^{-5}
650	760	500	13.3		
870	930	876	18.2		
1000	936	1000	19.8		
1200	1016	1500	26.3		
1400	1095	1655	28.3		
1655	1126	2126	37		
		2427	42		

Table 3 Temperature Dependent Elastic and Plastic Properties of Ti64

Temp. (°C)	Elastic		Plastic	
	Young's Modulus (GPa)	Poisson's Ratio	Yield Strength (MPa)	Plastic Strain
21	110	0.41	910	0.00
			1035	0.023
1655	11	0.45	91	0.00
			103.5	0.023

2.3 Thermal and Mechanical Loading

Thermal Model: The heat flux in the thermal model was applied using a DFLUX user subroutine in Abaqus Standard. The output of the heat flux (F) as a function of position (x) and time (t) was given by the following:

$$F = \frac{CP}{\pi r^2} e^{\frac{-2(x-vt)^2}{r^2}}$$

(1)

where C was the absorption factor, P was laser power in watts, r was the laser beam radius in meters, and v was the scanning speed of the heat flux [37]. The process parameters for the applied heat flux during selective laser melting are given in Table 4.

Table 4 Process Parameters for Applied Heat Flux during Selective Laser Melting

Laser power (W)	Scan speed (mm/s)	Layer thickness (µm)	Laser spot radius (µm)	Scan length (mm)
20	50	100, 300, 600	36	2

Stress Model: Laser peening was applied in the stress analysis after selective laser melting. To model laser shock peening, a simplified pressure load was applied to capture the highly transient, dynamic nature of a shock wave produced by plasma expansion. The laser spot size from peening was 500 µm. The pressure pulse was assumed to be 2-3 times longer than a typical 5-7 ns laser pulse [38,39]. The pressure pulse width was 20 ns, and the peak pressure was 1 GPa or 2 GPa. The peening pressure $P(r,t)$ as a function of both radial position and time was given by

$$P(r,t) = P(t)e^{\frac{-x^2}{2r^2}}$$

(2)

where $P(t)$ represents pressure at any time t, r is the radius of the laser spot [40]. Typically, the pressure pulse as a function of time has a Gaussian profile with a short rise time [38,41-43]. In this study, a simplified triangular pulse of the pressure as a function of time was used (Fig. 2). The pressure was applied in the center of the mesh.
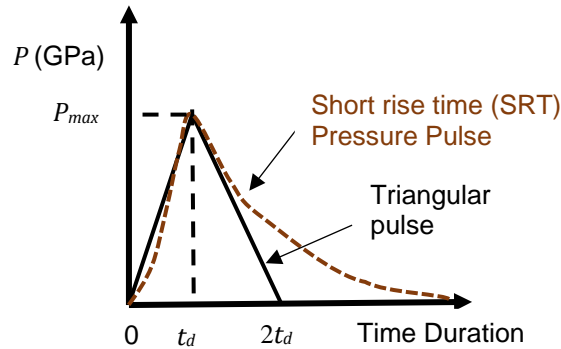

Fig. 2 Pressure-time history of a single pressure pulse from LSP.

2.4 Initial and Boundary Conditions

The initial temperature of the model was 20°C. During the stress analysis, the nodal temperatures were imported from the thermal model as a prescribed condition during the active heat flux step. Heat was allowed to conduct through the material. No heat transfer boundary conditions were prescribed. The displacement and rotation degrees of freedom along the bottom of the substrate were constrained in the analysis.

3. Results and Discussion

The temperature and stress fields are plotted along the depth direction at the center of the mesh, i.e. along Line A in Fig. 1. The temperature profiles are shown when the heat flux was directly over Line A. For the stress profiles, the heat flux passed over the layer and the stress S11 was plotted 0.1 ms after the pressure pulse.

3.1 Displacement

The magnitude of displacement (U) for a 100 µm, 300 µm, and 600 µm layer thickness exposed to a 1 GPa and 2 GPa peening pressure is shown in Fig. 3. It was observed that 1 GPa peening pressure did not cause severe plastic deformation. The maximum transient deformation was approximately 10 µm during peening. The maximum deformation after relaxation was approximately 2-3 µm. At 2GPa, the deformation was considerably higher. The deformation following relaxation was greater than 200 µm. Also, it was observed that deformation in 300 µm layer model was higher than in the 600 µm layer model. This may be attributed to the expansion during the thermal load varies depending on layer thickness and affects the deformation.
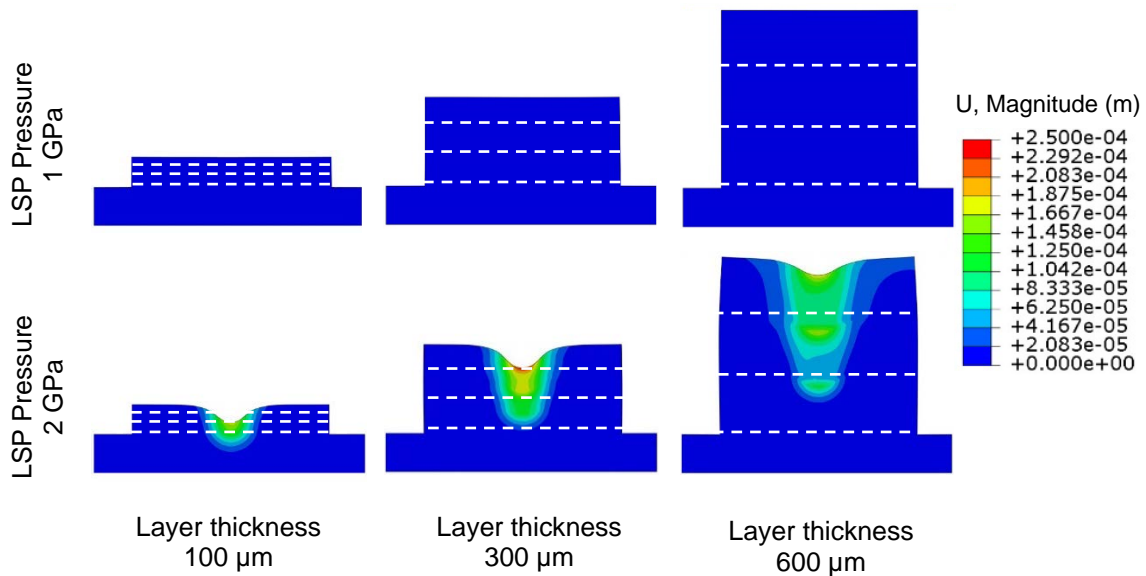

Fig. 3 Magnitude of deformation in a 100 µm, 300 µm, and 600 µm layer thickness model exposed to a 1 GPa and 2 GPa peening pressure.

3.2 Nodal Temperatures

Nodal temperatures from the applied heat flux for a 100 µm, 300 µm, and 600 µm layer thickness are shown in Fig. 4. The blue triangles represent the temperatures while printing layer 1, the red squares represent the temperature while printing layer 2, and the black circles represent the temperature while printing layer 3. In selective laser melting, the top surface is constantly changing by adding subsequent layers. Therefore, note that a zero depth corresponds to the top of layer 3. If the layer thickness is 100 µm (Fig. 4a), the top of layer 1 corresponds to a depth of 200 µm. For a 600 µm layer thickness (Fig. 4c), the top of layer 1 corresponds to a depth of 1200 µm.

The nodal temperatures exceeded 3000 °C on the top surface. For the given heat flux conditions, the results indicated that when the layer thickness was 100 µm (Fig. 4a), the temperature in layer 1 while printing layer 2 was between 800 °C and 1800 °C. The temperature

was relatively high considering that the solidus temperature of Ti64 was 1605 °C. This indicates that part of layer 1 was re-melted during the printing of layer 2. When printing layer 3, the temperature in layer 1 ranged from 200 °C to 600 °C.
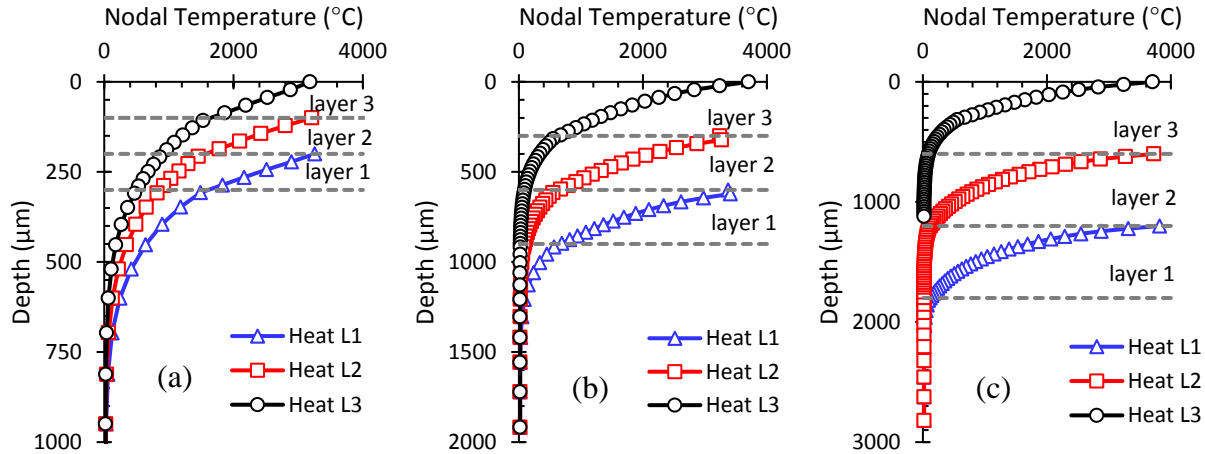

Fig. 4 Nodal temperatures (NT11) along the depth direction below applied heat flux for a (a) 100 µm, (b) 300 µm, and (c) 600 µm layer thickness.

When the layer thickness was 300 µm, the maximum temperature in layer 1 while printing layer 2 was approximately 450 °C. The maximum temperature in layer 1 while printing layer 3 was 75 °C. As the layer thickness increased to 600 µm, the temperatures in layer 1 while printing layer 2 was nearly room temperature. The results indicated that for the given heat flux in this study, the layer thickness needs to be greater than 300 µm to avoid significantly raising the temperature of previously laser peened layers. Models such as this can help determine the critical layer thickness for hybrid additive manufacturing processes so that thermal loads from SLM do not negate enhanced mechanical or physical properties in prior layers.

4.3 Residual Stress after LSP

The residual stress (S11) along the depth direction after laser shock peening with a pressure of 1 GPa (Fig. 5) and 2 GPa (Fig. 6) with a layer thickness of 100 µm, 300 µm, and 600 µm is shown below. For a layer thickness of 100 µm, 1 GPa was not significant enough to cause compressive residual stress in the printed layer, see Fig. 5a. The stress in each layer was a tensile and between 400 MPa and 800 MPa. When the pressure increased to 2 GPa (Fig. 6a), significant compressive residual stresses were imparted in layers 1, 2, and 3. When printing subsequent layers, e.g. layer 3, the heat flux caused the compressive stress from peening in layers 1 and 2 to turn tensile. The layer thickness was relatively small such that the thermal load from the subsequent layer's heat flux may be expanding the workpiece such that the compressive residual stresses are reversed. Furthermore, the higher pressure (2 GPa) coupled with such a thin layer resulted in layer 1 shifting to compression when layer 3 was peened.
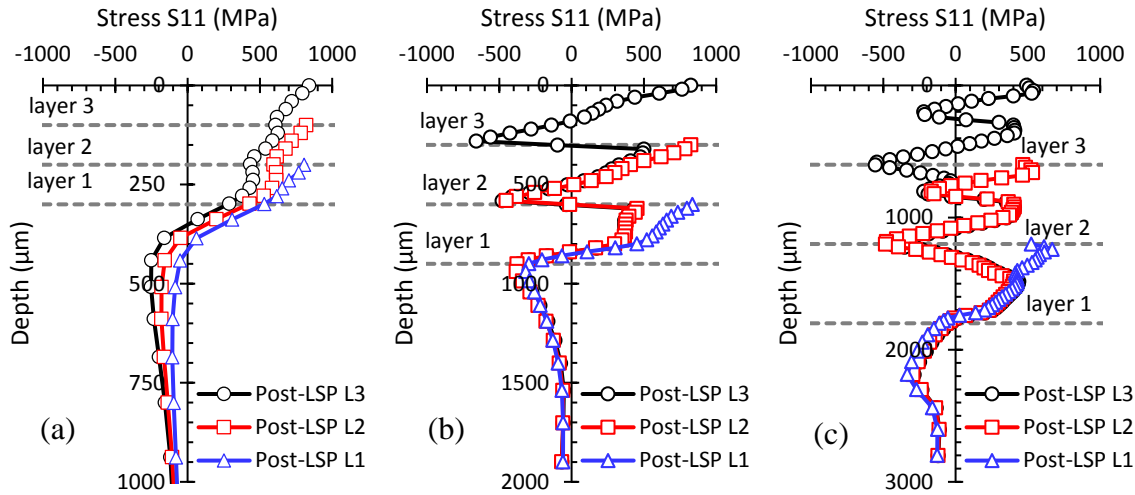
Fig. 5 S11 along the depth direction after laser peening with a pressure of 1 GPa for (a) 100 µm, (b) 300 µm, and (c) 600 µm layer thickness.
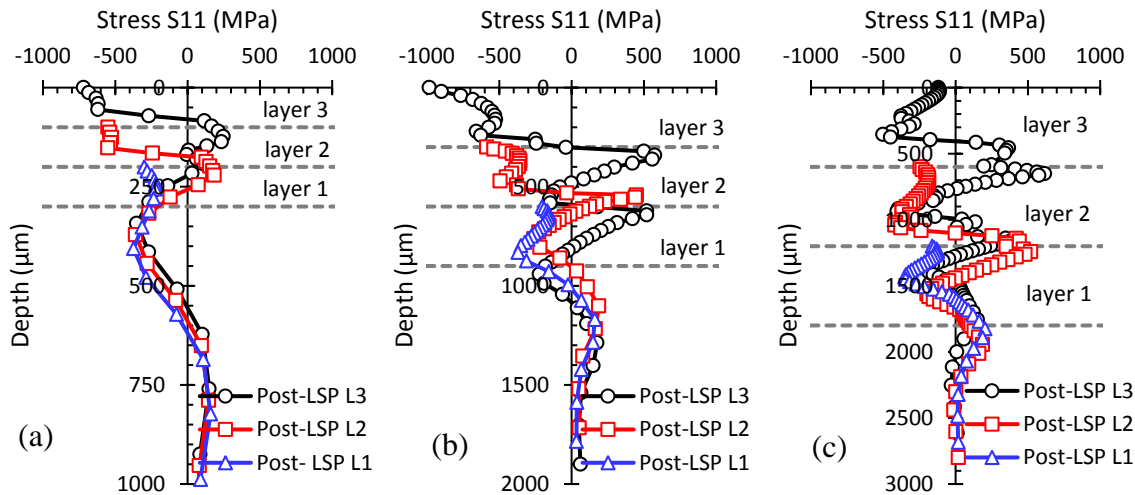
Fig. 6 S11 along the depth direction after laser peening with a pressure of 2 GPa for (a) 100 µm, (b) 300 µm, and (c) 600 µm layer thickness.

In the 300 µm layer thick model, a similar trend was observed. The high tensile stresses in between the layers were due to the fact that the heat flux from a subsequent layer caused significant thermal expansion and resulted in high tensile stresses. With 2 GPa peening pressures, the maximum compressive stress was more than 900 MPa. The tensile stresses in layer 1 developed during thermal loading of layer 2 remained tensile even after the peening layer 2.

Similarly, in the 600 µm layer thick model, the tensile stresses joining two layers were due to the thermal loads and the compressive stresses within the layers were due to peening. The compressive stresses were not as high as those in the 300 µm layer thick model because all of the

heat energy accumulated in one thick layer. Significant thermal expansion ensued and led to tensile stresses on the order of 500 MPa. Subsequent peening did not have a significant effect because the layers were much thicker.

The maximum tensile stresses occurred at the boundary between layers. This was due to an excessive amount of thermal expansion during thermal loading and the fact that layers were added as plates on one another. In reality, the starting material in SLM is powder which would be deposited and melted to the substrate. In that case, there should be less thermal expansion than what was observed in a plate.

5. Summary and Conclusions

This work presents a finite element model of a hybrid additive manufacturing process that couples selective laser melting (SLM) and laser shock peening (LSP). The model adds a new layer that is subsequently laser peened. The process is repeated for three layers. The objective was to quantify the effects of single shot LSP after printing multiple layers. In other words, how does the thermal load from subsequent printed layers influence the residual stress imparted by LSP in prior layers? The effects of laser peening pressure and layer thickness on the residual stress fields were analyzed. This model established the fact that layer thickness plays a critical role on the resulting residual stress fields. If a layer is thicker than a critical value, the thermal loads from printing more layers will not significantly alter the residual stress field in previous layers. For thinner layers, more substantial pressures are needed to cause deeper compressive residual stresses. The results suggest that peening conditions can eventually be optimized to have the desired residual stress contour for a given application. Further studies are needed to incorporate microstructural evolution from hybrid printing multiple layers in a model.

6. References

[1]   M. Shiomi, K. Osakada, K. Nakamura, T. Yamashita, F. Abe, Residual Stress within Metallic Model Made by Selective Laser Melting Process, CIRP Ann. Manuf. Technol. 53 (2004) 195-198.

[2]   B. Lauwers, F. Klocke, A. Klink, A.E. Tekkaya, R. Neugebauer, D. Mcintosh, Hybrid processes in manufacturing, CIRP Ann. Manuf. Technol. 63 (2014) 561-583.

[3]   J.M. Flynn, A. Shokrani, S.T. Newman, V. Dhokia, Hybrid additive and subtractive machine tools – Research and industrial developments, Int. J. Mach. Tools Manuf. 101 (2016) 79-101.

[4]   J. Jeng, M. Lin, Mold fabrication and modification using hybrid processes of selective laser cladding and milling, J. Mater. Process. Technol. 110 (2001) 98-103.

[5]   J.P-. Kruth, M.C. Leu, T. Nakagawa, Progress in Additive Manufacturing and Rapid Prototyping, CIRP Ann. Manuf. Technol. 47 (1998) 525-540.

[6]   G.N. Levy, R. Schindel, J.P. Kruth, Rapid Manufacturing and Rapid Tooling with Layer Manufactuirng (LM) Technologies, State of the Art and Fututre Perspectives, CIRP Ann. Manuf. Technol. 52 (2003) 589-609.

[7]   K.P. Karunakaran, P.V. Shanmuganathan, S.J. Jadhav, P. Bhadauria, A. Pandey, Rapid prototyping of metallic parts and moulds, J. Mater. Process. Technol. 105 (2000) 371-381.

[8]   K.P. Karunakaran, S. Suryakumar, V. Pushpa, S. Akula, Low cost integration of additive and subtractive processes for hybrid layered manufacturing, Robot. Comput. Integrated Manuf. 26 (2010) 490-499.

[9]   J. Hur, K. Lee, Zhu-hu, J. Kim, Hybrid rapid prototyping system using machining and deposition, Comput. -Aided Des. 34 (2002) 741-754.

[10] F. Liou, K. Slattery, M. Kinsella, J. Newkirk, H.N. Chou, R. Landers, Applications of Hybrid Manufacturing Process for Fabrication and Repair of Metallic Structures, AFRL-ML-WP-TP-2006-444. (2006) 1-11.

[11] K.A. Lorenz, J.B. Jones, D.I. Wimpenny, M.R. Jackson, A Review of Hybrid Manufacturing, International Solid Freeform Fabrication Symposium, Austin, Texas. (2015) 96-108.

[12] J.K.S. Nagel, F.W. Liou, Hybrid Manufacturing System Design and Development, Manufacturing Systems (F. Aziz), InTech. (2012) 223-246.

[13] P.A. Colegrove, F. Martina, M.J. Roy, B.A. Szost, S. Terzi, S.W. Williams, P.J. Withers, D. Jarvis, High Pressure Interpass Rolling of Wire + Arc Additively Manufactured Titanium Components, Advanced Materials Research. 996 (2014) 694-700.

[14] F. Martina, P.A. Colegrove, S.W. Williams, J. Meyer, Microstructure of Interpass Rolled Wire + Arc Additive Manufacturing Ti-6Al-4V Components, Metallurgical and Materials Transactions A. 46 (2015) 6103-6118.

[15] Y. Xie, H. Zhang, F. Zhou, Improvement in Geometrical Accuracy and Mechanical Property for Arc-Based Additive Manufacturing Using Metamorphic Rolling Mechanism, Journal of Manufacturing Science and Engineering. 138 (2016) 111002-111002.

[16] X. Zhou, H. Zhang, G. Wang, X. Bai, Y. Fu, J. Zhao, Simulation of microstructure evolution during hybrid deposition and micro-rolling process, J. Mater. Sci. 51 (2016) 6735-6749.

[17] E. Yasa, J.-. Kruth, J. Deckers, Manufacturing by combining Selective Laser Melting and Selective Laser Erosion/laser re-melting, CIRP Ann. Manuf. Technol. 60 (2011) 263-266.

[18] E. Yasa, J. Deckers, J.P. Kruth, The investigation of the influence of laser re-melting on density, surface quality and microstructure of selective laser melting parts, Rapid Prototyping Journal. 17 (2011) 312-327.

[19] J. Ramos-Grez, D.L. Bourell, Reducing surface roughness of metallic freeform-fabricated parts using non-tactile finishing methods, International Journal of Materials and Product Technology. 21 (2004) 297-316.

[20] S. Akula, K.P. Karunakaran, Hybrid adaptive layer manufacturing: An Intelligent art of direct metal rapid tooling process, Robot. Comput. Integrated Manuf. 22 (2006) 113-123.

[21] Y. Qian, H. Zhang, G. Wang, Research of rapid and direct thick coatings deposition by hybrid plasma-laser, Appl. Surf. Sci. 252 (2006) 6173-6178.

[22] Y. Song, S. Park, Experimental investigations into rapid prototyping of composites by novel hybrid deposition process, J. Mater. Process. Technol. 171 (2006) 35-40.

[23] M. Ono, Y. Shinbo, A. Yoshitake, M. Ohmura, Development of laser-arc hybrid welding, NKK Technical Report - Japanese Edition. (2002) 70-74.

[24] G. Campana, A. Fortunato, A. Ascari, G. Tani, L. Tomesani, The influence of arc transfer mode in hybrid laser-mig welding, J. Mater. Process. Technol. 191 (2007) 111-113.

[25] Y. Sano, N. Mukai, K. Okazaki, M. Obata, Residual stress improvement in metal surface by underwater laser irradiation, Nuclear Instruments and Methods in Physics Research Section B: Beam Interactions with Materials and Atoms. 121 (1997) 432-436.

[26] W. Zhang, Y.L. Yao, Micro Scale Shock Processing of Metallic Components, Journal of Manufacturing Science and Engineering. 124 (2002) 369-378.

[27] W. Braisted, R. Brockman, Finite element simulation of laser shock peening, Int. J. Fatigue. 21 (1999) 719-724.

[28] Z. Yongkang, Z. Shuyi, Z. Xiaorong, C. Lan, Y. Jichang, R. Naifei, Investigation of the surface qualities of laser shock-processed zones and the effect on fatigue life of aluminum alloy, Surface and Coatings Technology. 92 (1997) 104-109.

[29] P. Mercelis, Jean-Pierre Kruth, Residual stresses in selective laser sintering and selective laser melting, Rapid Prototyping Journal. 12 (2006) 254-265.

[30] M.P. Sealy, Y.B. Guo, Fabrication and Finite Element Simulation of Micro-Laser Shock Peening for Micro Dents, Int. J. Comp. Meth. Eng. Sci. Mech. 10 (2009) 134-142.

[31] M.P. Sealy, Y.B. Guo, Surface integrity and process mechanics of laser shock peening of novel biodegradable magnesium–calcium (Mg–Ca) alloy, J. Mech. Behav. Biomed. Matrl. 3 (2010) 488-496.

[32] C.H. Fu, Y.B. Guo, 3-Dimensionl Finite Element Modeling of Selective Laser Melting Ti-6Al-4V Alloy, 2014 Inter. Solid Freeform Fabrication Symposium. (2014) 1129-1144.

[33] M. Boivineau, C. Cagran, D. Doytier, V. Eyraud, M.-. Nadal, B. Wilthan, G. Pottlacher, Thermophysical Properties of Solid and Liquid Ti-6Al-4V (TA6V) Alloy, Int. J. Thermophys. 27 (2006) 507-529.

[34] F. Verhaeghe, T. Craeghs, J. Heulens, L. Pandelaers, A pragmatic model for selective laser melting with evaporation, Acta Materialia. 57 (2009) 6006-6012.

[35] R. Boyer, G. Welsch, E.W. Collings, Materials Properties Handbook: Titanium Alloys, ASM International, 1993.

[36] P. Edwards, M. Ramulu, Fatigue performance evaluation of selective laser melted Ti–6Al–4V, Materials Science and Engineering: A. 598 (2014) 327-337.

[37] I.A. Roberts, C.J. Wang, R. Esterlein, M. Stanford, D.J. Mynors, A three-dimensional finite element analysis of the temperature field during laser melting of metal powders in additive layer manufacturing, Int. J. Mach. Tools Manuf. 49 (2009) 916-923.

[38] D. Devaux, R. Fabbro, L. Tollier, E. Bartnicki, Generation of shock waves by laser-induced plasma in confined geometry, J. Appl. Phys. 74 (1993) 2268-2273.

[39] L. Berthe, R. Fabbro, P. Peyre, E. Bartnicki, Wavelength dependent of laser shock-wave generation in the water-confinement regime, J. Appl. Phys. 85 (1999) 7552-7555.

[40] A.H. Clauer, Laser Shock Peening for fatigue resistance, Surface Performance of Titanium (1996) 217-230.

[41] L. Berthe, R. Fabbro, P. Peyre, L. Tollier, E. Bartnicki, Shock waves from a water-confined laser-generated plasma, J. Appl. Phys. 82 (1997) 2826-2832.

[42] R. Fabbro, J. Fournier, P. Ballard, D. Devaux, J. Virmont, Physical study of laser-produced plasma in confined geometry, J. Appl. Phys. 68 (1990) 775-784.

[43] B. Wu, Y.C. Shin, A self-closed thermal model for laser shock peening under the water confinement regime configuration and comparisons to experiments, J. Appl. Phys. 97 (2005) 113517:1-11.